MCB
Journals.ASM.org

Substrate Trapping Proteomics Reveals Targets of the βTrCP2/FBXW11 Ubiquitin Ligase

Tai Young Kim,[a,b*] Priscila F. Siesser,[a,b] Kent L. Rossman,[b,c] Dennis Goldfarb,[a,d] Kathryn Mackinnon,[a,b] Feng Yan,[a,b] XianHua Yi,[e] Michael J. MacCoss,[e] Randall T. Moon,[f] Channing J. Der,[b,c] Michael B. Major[a,b,d]

Department of Cell Biology and Physiology,[a] Lineberger Comprehensive Cancer Center,[b] Department of Pharmacology,[c] and Department of Computer Science,[d] University of North Carolina at Chapel Hill, Chapel Hill, North Carolina, USA; Department of Genome Sciences[e] and Department of Pharmacology and HHMI,[f] University of Washington, Seattle, Washington, USA

Defining the full complement of substrates for each ubiquitin ligase remains an important challenge. Improvements in mass spectrometry instrumentation and computation and in protein biochemistry methods have resulted in several new methods for ubiquitin ligase substrate identification. Here we used the parallel adapter capture (PAC) proteomics approach to study βTrCP2/FBXW11, a substrate adaptor for the SKP1–CUL1–F-box (SCF) E3 ubiquitin ligase complex. The processivity of the ubiquitylation reaction necessitates transient physical interactions between FBXW11 and its substrates, thus making biochemical purification of FBXW11-bound substrates difficult. Using the PAC-based approach, we inhibited the proteasome to "trap" ubiquitylated substrates on the SCF^{FBXW11} E3 complex. Comparative mass spectrometry analysis of immunopurified FBXW11 protein complexes before and after proteasome inhibition revealed 21 known and 23 putatively novel substrates. In focused studies, we found that SCF^{FBXW11} bound, polyubiquitylated, and destabilized RAPGEF2, a guanine nucleotide exchange factor that activates the small GTPase RAP1. High RAPGEF2 protein levels promoted cell-cell fusion and, consequently, multinucleation. Surprisingly, this occurred independently of the guanine nucleotide exchange factor (GEF) catalytic activity and of the presence of RAP1. Our data establish new functions for RAPGEF2 that may contribute to aneuploidy in cancer. More broadly, this report supports the continued use of substrate trapping proteomics to comprehensively define targets for E3 ubiquitin ligases. All proteomic data are available via ProteomeXchange with identifier PXD001062.

Ubiquitylation is a posttranslational modification that controls protein-protein interactions, protein subcellular localization, protein-mediated catalysis, and, most famously, protein stability. The enzymology of protein ubiquitylation is now fairly well understood and has been well summarized in several recent reviews (1–3). The last and arguably most important step in the ubiquitylation reaction is carried out by an E3 ubiquitin ligase. These proteins select substrates for ubiquitylation, physically bridge and orient the substrate with ubiquitin, and in some cases, directly catalyze ubiquitin transfer. E3 ligases also provide the cell with a means to dynamically regulate substrate ubiquitylation; the interaction of a substrate protein with its cognate E3 ligase is often influenced by peripheral signals, such as phosphorylation (4). In total, more than 600 distinct E3 ubiquitin ligases have been identified within the human genome (5), the vast majority of which remain unstudied. Current estimates suggest that these ligases target more than 9,000 distinct human proteins for ubiquitylation, or roughly 40% of the protein-coding human genome (6, 7). For most of these proteins, the physiological importance of ubiquitin conjugation is not known. Likewise, paired relationships between specific E3 ligases and substrates are for the most part not known.

Until recently, substrate identification for specific ubiquitin ligase complexes has been a major hurdle for the ubiquitylation community (reviewed in reference 8). Focused biochemical and genetic studies have succeeded in revealing substrates but have done so for only a small number of well-studied ligases. The difficulty lies in the transient nature of the E3-substrate interaction and in the often low cellular abundance of substrate protein. Consequently, substrates are often missed in biochemical analyses of immunopurified E3 complexes. New experimental approaches are beginning to overcome this problem (8–10). Short-term treatment of cells with inhibitors of the ubiquitylation cycle results in substrate stabilization and, importantly, accumulation of the substrate-E3 complex. This has previously been achieved with small molecules that block the proteasome or cullin neddylation (11–13). Consequently, protein mass spectrometry (MS) analysis of the immunopurified ligase complex before and after proteasome or NEDD8 inhibition reveals the identity and quantity of trapped substrates; this approach was recently termed parallel adaptor capture proteomics (PAC) (13). Similarly, purification of mutant E3 adapter proteins, where the engineered mutation blocks substrate turnover but not substrate binding, revealed known and novel substrates (14). Taking an *in vitro* approach, Michele Pagano and colleagues have used immunoprecipitated E3 protein complexes and exogenous epitope-tagged ubiquitin to identify

Received 27 June 2014 **Returned for modification** 24 July 2014
Accepted 11 October 2014

Accepted manuscript posted online 20 October 2014

Citation Kim TY, Siesser PF, Rossman KL, Goldfarb D, Mackinnon K, Yan F, Yi X, MacCoss MJ, Moon RT, Der CJ, Major MB. 2015. Substrate trapping proteomics reveals targets of the βTrCP2/FBXW11 ubiquitin ligase. Mol Cell Biol 35:167–181. doi:10.1128/MCB.00857-14.

Address correspondence to Michael B. Major, ben_major@med.unc.edu.

* Present address: Tai Young Kim, College of Pharmacy, Seoul National University, Seoul, Republic of Korea.

T.Y.K. and P.F.S. contributed equally to this article.

Supplemental material for this article may be found at http://dx.doi.org/10.1128/MCB.00857-14.

doi:10.1128/MCB.00857-14

numerous novel ubiquitylated substrates (10, 15, 16). Two additional discovery platforms provide powerful complementation of these substrate identification approaches. First, ubiquitin remnant proteomic analyses performed via immunopurification of Lys-ε-Gly-Gly (diGly) modified peptides and mass spectrometry revealed global proteome ubiquitylation (17). Second, the Global Protein Stability (GPS) platform quantifies dynamic changes in protein stability following genetic perturbation of specific ubiquitylation machinery (18, 19). Proteins identified through either diGLY or GPS analysis should be enriched within PAC-derived interaction networks.

Here, we have taken a PAC-based approach to identify substrates for the βTrCP2/FBXW11 E3 ubiquitin ligase. FBXW11 and its related paralogue βTrCP1/BTRC are F-box domain-containing proteins that serve as substrate adaptor proteins within SKP1- and CUL1-containing E3 ubiquitin ligase complexes; together, these proteins constitute SCF^{FBXW11} or SCF^{BTRC}. FBXW11 and BTRC are among the best-studied E3 proteins, with at least 30 identified substrates and well-described roles in controlling cell cycle and signal transduction (20). Using substrate trapping proteomic analysis of FBXW11, we identified 21 previously reported substrates and 23 novel candidate substrates. These data and recent PAC-based proteomic studies suggest that, despite more than a decade of research, the full complement of FBXW11 and BTRC substrates is not yet known.

This report focuses on a new FBXW11 substrate, RAPGEF2 (also called PDZ-GEF1, RA-GEF1, nRAPGEF, and CNrasGEF). RAPGEF2 is a guanine nucleotide exchange factor (GEF) for the RAP1 and RAP2 (RAP1/2) small GTPases (21). In addition to a C-terminal RAPGEF catalytic CDC25 homology domain, RAPGEF2 contains amino-terminal cNMP, PDZ, and RA domains. RAP protein activity is governed by nucleotide binding; GEFs catalyze the exchange of GDP for GTP, thus promoting formation of active RAP. Conversely, GTPase activating proteins (GAP) trigger the hydrolysis of GTP to GDP and formation of inactive RAP-GTP (22). Genetic studies in *Caenorhabditis elegans*, *Drosophila*, and mice describe vital functions for RAPGEF2 in controlling RAP1-dependent modulation of the actin cytoskeleton, leading to decreased cell adhesion, cell polarity, cell-cell contacts, and cell migration (23–25). Mice deficient for RAPGEF2 display multiple developmental defects, including reduced vascular barrier formation (26). A role for RAPGEF2 in cancer, albeit complex and tissue specific, has also emerged. First, a murine piggyBac insertional mutagenesis screen identified RAPGEF2 and its associated protein MAGI1 as "driver" genes in melanoma (27). Second, RAPGEF2 controls the migratory capacity of multiple cell types. For example, its expression inhibited breast cancer cell migration *in vitro* and suppressed cell invasion/metastasis in a zebrafish xenograft model (28). Third, RAPGEF2 activation of RAP1 in turn activated B-Raf and the extracellular signal-regulated kinase (ERK) mitogen-activated protein kinase cascade in multiple cell types, including neurons and endocrine cells (29). Together, these and many other reports describe evolutionarily conserved and fundamental roles for RAPGEF2 in development and disease.

Using PAC-based proteomic analysis, we discovered known and novel substrates for FBXW11, including RAPGEF2, TBC1D4, STK3, RASSF3, and AEBP2. Our focused experiments confirm and extend recent findings that RAPGEF2 is a physiologically important substrate for FBXW11 (28). We report a GEF activity- and RAP1-independent function for RAPGEF2 in promoting cellular multinucleation which, remarkably, occurs through cell-cell fusion events.

MATERIALS AND METHODS

Expression vectors and site-directed mutagenesis. The FLAG-RAPGEF2 and YFP-RAPGEF2 expression vectors were generous gifts from Lawrence Quillam (Indiana University) and Johannes L. Bos (University Medical Centre Utrecht, Netherlands), respectively. The hemagglutinin (HA)-ubiquitin expression plasmid was a gift from Yue Xiong, University of North Carolina at Chapel Hill. The three truncation mutations (RAPGEF2-Δ1, -Δ2, and -Δ3) and a point mutation (RAPGEF2-2SA) were generated by PCR-based mutagenesis using *Pfu* DNA polymerase. The sense primer sequence for the point mutation is as follows: 5′-TGA TGC TGC TGA CGC TGG C CG TGG GGC CTG GAC GTC ATG CT-3′. A GEF-dead mutant of RAPGEF was generated by sequential PCRs to generate YFP-RAPGEF2 (K875A/F879A/N884A; 3M). The double point mutation (F879A/N884A) was first created using the following sense primer: 5′-AAA G GA TCT CAC CGC CCT TCA CGA AGG AGC TGA CTC AAA AGT AG-3′. The triple point mutation (K875A/F879A/N884A) was then generated using the F879A/N884A construct as a template and the following sense primer: 5′-CTA TTC CCA GTT ATC AAA GCG GAT CTC ACC GCC CTT CAC-3′. The presence of point mutations was verified by DNA sequencing. Generation and characterization of the SBPHA-BTRC, SBPHA-FBXW11, SBPHA-$CTNNB1^{SA}$, FLAG-BTRC, and FLAG-FBXW11 expression vectors were previously reported (30).

Cell culture, transfections, and siRNAs. HEK293 cells were maintained in Dulbecco's modification of Eagle's medium (DMEM) supplemented with 10% fetal bovine serum (FBS; HyClone) in a 37°C humidified incubator with 5% CO_2. Transfection of expression plasmids was done with Lipofectamine 2000 (Invitrogen) or Transit (Myrus), while transfection of small interfering RNA (siRNA) was done with Lipofectamine RNAiMAX, as directed by the manufacturer's instructions. All siRNAs were used at a final concentration of 20 nM and for 72 h unless otherwise stated. siRNA sequences were as follows: for BTRC/FBXW11 (this siRNA targets identical sequences in BTRC and FBXW11), GUG GAA UUU GUG GAA CAU C deoxyribosylthymine (dT) dT; for RAPGEF2-A, CAG UGG AAC CUU AUC AUC CAG UAA U; for RAPGEF2 B, GGG UGG AAA GGA UGU UUC CAU UGA A; for NEDD4-A, GGA UAA ACU UCA GAU GGC AAU UGA A; and for NEDD4-B, GGA UCA GAA AUA GUU GUC ACC AAU A. Nontargeting control siRNA was obtained from Dharmacon and Invitrogen. Generation of monoclonal cells stably expressing RAPGEF2 was achieved by Lipofectamine transfection of HEK293 cells with YFP-RAPGEF2 plasmid, followed by fluorescence-activated cell sorter analysis (FACS) of yellow fluorescent protein (YFP)-positive single cells on a 96-well plate and expansion of monoclonal populations.

Western blotting and immunoprecipitation. In all biochemical experiments, cell lysates were prepared in a buffer containing 50 mM Tris-HCl (pH 7.5), 150 mM NaCl, 1% NP-40, 10 mM NaF, 5 mM EDTA, and protease and phosphatase inhibitor cocktail (Roche). For immunoprecipitation, equal amounts of precleared cell lysates were incubated with 1 μg of the indicated antibody or control IgG overnight. Protein A/G-Sepharose beads (GE Healthcare) were added to each of the samples, and the reaction mixtures were further incubated for 2 to 3 h and washed three times. Bound proteins were eluted from the beads with SDS-PAGE sample buffer, and Western blotting was performed with the following antibodies: anti-FLAG M2 monoclonal (Sigma-Aldrich Corporation), anti-HA monoclonal (MMS-101P; Covance), anti-green fluorescent protein (anti-GFP) polyclonal (ab290; Abcam), anti-RAPGEF2 polyclonal (A301-966A; Bethyl Laboratories), anti-Rap1 polyclonal (sc-65; Santa Cruz Biotechnology), anti-BTRC (D13F10; Cell Signaling Technology), anti-BTRC/FBXW11 (37-3400; Invitrogen), anti-CTNNB1 polyclonal (9562; Cell Signaling Technology), anti-NEDD4 (3606; Cell Signaling Technol-

ogy), USP47 (A301-048A; Bethyl Laboratories), DOCK1 (sc-13163; Santa Cruz Biotechnology), NUDC (10681-1-AP; ProteinTech Group), DAP3 (H00007818-A01; Abnova), STK3 and STK4 (STK3/4) (A300-466A; Bethyl Laboratories), TBC1D4 (ab24469; Abcam), SKP1 (2156; Cell Signaling Technology), anti-β-tubulin monoclonal (T7816; Sigma-Aldrich), and antiactin polyclonal (A2066; Sigma-Aldrich) (recognizes α, β, and γ) antibodies.

Protein identification. FLAG immunoprecipitation, trypsinization, and mass spectrometry were performed exactly as previously reported (31). SBP_CBP-based tandem affinity purification and mass spectrometry (TAPMS) were performed as previously described (32). The peptide mixture was analyzed in positive mode using a nanoAquity ultraperformance liquid chromatography (UPLC)-coupled LTQ Orbitrap Elite mass spectrometer (Thermo Scientific). Chromatographic separation used a 2-cm-long trapping column and a self-packed 25-cm-long analytical column (75 μm inner diameter [ID]) and Michrom Magic C18 beads of 5.0-μm particle diameter and 100-Å pore diameter. The HPLC flow rate was set to 350 nl/min over a gradient of 1% buffer B (0.1% formic acid–acetonitrile) to 35% buffer B in 200 min. The full mass scan (300 to 2,000 *m*/*z*) was acquired at a resolution of 60,000 with a maximum injection time of 500 ms, and tandem MS (MS/MS) was performed in a data-dependent manner for the top 15 ions exhibiting the greatest intensity in the linear ion trap by collision-induced dissociation. All raw spectral data were converted to mzXML format before a search of the resultant spectra with Sorcerer-SEQUEST (build 4.3.0; Sage-N Research) and the Trans-Proteomic Pipeline (TPP v4.6.2) was performed. Data were searched against the human UniProtKB/Swiss-Prot sequence database (Release 2013_07) supplemented with common contaminants, such as porcine (Swiss-Prot P00761) and bovine (P00760) trypsin, and further concatenated with the reversed copy of each sequence as a decoy (40,526 total sequences). Search parameters used were a precursor mass between 400 and 4,500 atomic mass units (amu), up to two missed cleavages, a precursor-ion tolerance of three amu, accurate mass binning within PeptideProphet (33), semitryptic digestion, a static carbamidomethyl cysteine modification, and variable methionine oxidation. False-discovery rates (FDRs) were determined by ProteinProphet (33), and minimum protein probability cutoffs resulting in a 1% FDR were selected individually for each experiment. The mass spectrometry proteomics data have been deposited into the ProteomeXchange Consortium (34) via the PRIDE partner repository with the data set identifier PXD001062.

Bioinformatics. PeptideProphet/ProteinProphet results for each APMS experiment were stored in a local Prohits database (35). Candidate protein interactions from APMS experiments were filtered using the CompPASS algorithm. FLAG and TAPMS background data sets required for CompPASS were obtained from previous experiments performed by our laboratory. Experiments performed with MG132 or dimethyl sulfoxide (DMSO) treatment were scored separately from each other. Network visualization was achieved using Cytoscape v3.1.0 (36). Known protein-protein interactions were extracted from the 04/2014 build of BioGRID. Multiple-sequence alignment for analysis of a short amino acid motif in substrate proteins referred to as a degron was performed using GLAM2 and GLAM2SCAN (37).

***In vivo* ubiquitylation assays.** HEK293 cells were transfected with plasmids expressing FLAG-RAPGEF2 and HA-ubiquitin for 24 h and treated with DMSO or 10 μM MG132 for 6 h. For BTRC/FBXW11 knockdown, control or BTRC/FBXW11 siRNAs were transfected 24 h prior to plasmid transfection. The cells were lysed with SDS lysis buffer (50 mM Tris-HCl at pH 8.0, 100 mM NaCl, 2% Triton X-100, 1% SDS) and boiled for 10 min. Lysates were then diluted 10× with NP-40 buffer (50 mM Tris-HCl at pH 7.5, 150 mM NaCl, 0.5% NaCl, 50 mM NaF). The diluted lysates were applied to immunoprecipitation with anti-M2 FLAG affinity gel (Sigma). The immunoprecipitated proteins were analyzed by Western blotting with anti-HA antibody for the detection of ubiquitin-conjugated RAPGEF2.

RAP1 activity assay. RAP1 activity was examined by a pulldown method using a glutathione *S*-transferase (GST) fusion of an isolated RAP-GTP binding domain (RBD) of RalGDS (GST-RalGDS-RBD) as described previously (38). Briefly, HEK293 cells plated in a 60-mm-diameter culture dish were transfected with 3 μg of empty plasmid (Mock), RAPGEF2 (wild type [WT]), or RAPGEF2 (K875A/F879A/N884A; 3M) for 24 to 36 h, lysed in 300 μl of ice-cold cell lysis buffer (50 mM Tris-HCl [pH 7.5], 150 mM NaCl, 1% NP-40, 5 mM $MgCl_2$, 10% glycerol, protease inhibitor cocktail), and clarified by centrifugation at 14,000 rpm for 10 min at 4°C. A 5% aliquot was removed for determination of the total quantities of the RAP1 being analyzed. Cleared lysates were then incubated with 30 μg of GST-RalGDS (RBD) protein precoupled to glutathione-Sepharose 4B beads for 1 h at 4°C and washed three times with the lysis buffer. The samples were analyzed by immunoblotting using anti-RAP1 antibody to detect bound activated RAP1-GTP. Whole-cell lysates were also analyzed for the presence of expressed RAP1.

Immunofluorescence. For cell staining, HEK293 cells were plated on fibronectin-coated coverslips and allowed to attach and spread at 37°C in complete growth medium. Cells were transfected with the plasmids or siRNAs of interest and fixed 24 to 72 h after transfection as indicated. Fixation was performed with 4% paraformaldehyde (PFA; Electron Microscopy Sciences)–cytoskeletal buffer {5 mM PIPES [piperazine-*N*,*N*′-bis(2-ethanesulfonic acid)] (pH 6), 137 mM NaCl, 5 mM KCl, 1.1 mM sodium phosphate buffer, 0.4 mM KH_2PO_4, 0.4 mM $MgCl_2$, 0.4 mM $NaHCO_3$, 2 mM EGTA, 50 mM glucose} for 15 min and permeabilization with 0.1% Triton X-100–phosphate-buffered saline (PBS) for 5 min. After being blocked in 1% bovine serum albumin–PBS for 1 h, cells were incubated with primary antibodies at 4°C overnight, followed by incubation with appropriate secondary antibodies, Rhodamine Red X (RRX)-conjugated donkey anti-mouse immunoglobulin G (IgG), fluorescein isothiocyanate-conjugated donkey anti-mouse IgG, and Cy5-conjugated donkey anti-goat antibody (Jackson ImmunoResearch Laboratories), at room temperature for 2 h. The following antibodies were used: monoclonal anti-α-tubulin (clone DM1A [T9026]; Sigma-Aldrich Corporation), monoclonal anti-CTNNB1 (BD Transduction Laboratories), and goat IgG anti-lamin B (Santa Cruz). Coverslips were mounted to slides with ProLong Gold antifade reagent containing DAPI (4′,6-diamidino-2-phenylindole; Invitrogen) for nuclear staining. Staining was analyzed with an Olympus BX61 upright wide-field microscope (Olympus Corporation of the Americas) equipped with 40×/1.3-numerical aperture (NA) oil UPlanFLN and 60×/1.42-NA oil PlanApo objective lenses and a Hamamatsu Orca RC camera (Hamamatsu Photonics Ltd.). For analysis of mitotic spindles, samples were processed as described above and analyzed with a Zeiss CLSM 700 confocal laser scanning microscope equipped with a 63×/1.4-NA PlanApo oil objective lens. Image processing was performed with ImageJ and Adobe Photoshop CS software.

Flow cytometry. HEK293 cells were transiently transfected with WT-RAPGEF2 or dead-RAPGEF2 or mock transfected, harvested after 48 h by using trypsin-EDTA, and resuspended in 10% FBS–DMEM. Cells (1.5×10^6) were fixed in 70% ethanol, treated with RNase A, and stained with 20 μg/ml propidium iodide for analysis of DNA content using a CyAn ADP analyzer (Beckman Coulter). Sequential gating was done to exclude cell debris, aggregates, and nontransfected cells. Percentages of cells in the G_0/G_1, S, and G_2/M stages of the cell cycle were determined by using ModiFit (Verity Software House, Topsham, ME). A total of 30,000 events were acquired for each of three replicate biological experiments.

Live cell imaging. HEK293 cells were transfected with YFP-WT-RAPGEF2 or cotransfected with YFP-WT-RAPGEF2 and cherry-nuclear localization signal (cherry-NLS) and imaged the next day. Time-lapse phase-contrast and fluorescence images were acquired every 6 min for 10 h with an Olympus IX70 inverted fluorescence microscope enclosed within an environmental chamber controlled for temperature, relative humidity, and CO_2 and equipped with 10×/0.30-NA Ph1 UPlanFL and 20×/0.40-NA Ph1 LCPlanFL objective lenses and a Hamamatsu Orca C4742-95 charge-coupled device camera. Data acquisition was carried out

with Volocity (version 5.5.1; PerkinElmer), and image processing was performed with ImageJ and Adobe Photoshop CS software.

RESULTS

Identification of FBXW11 substrates by APMS. The FBXW11 and BTRC protein-protein interaction networks were defined in HEK293T human embryonic kidney cells by tandem affinity purification and mass spectrometry (TAPMS). HEK293T cells were engineered to stably express FBXW11 or BTRC amino terminally tagged with streptavidin binding peptide (SBP), calmodulin binding peptide (CBP), and hemagglutinin (HA) epitope. The resulting cell lines were solubilized in duplicate biological experiments using 0.1% NP-40 or 1% Triton X-100 before TAPMS analysis. After removing false-positive interactions with the CompPASS algorithm (39), FBXW11 and BTRC were found to interact with 96 and 26 proteins, respectively (Fig. 1A). Twenty proteins cocomplexed with both FBXW11 and BTRC baits. Previously unstudied interacting proteins included NUDC, OGT, DOCK1, and ELMO2. As expected from their instability and transient interactions with the E3 enzyme, many previously reported substrates, including ATF4, NFKB1, PER1, and WEE1, were not identified. Therefore, the purifications were repeated before and after a 4-h treatment with MG132 proteasome inhibitor, in replicate biological experiments. Label-free quantitation and ratiometric analysis revealed associated proteins that increased in abundance within the FBXW11 complex following proteasome inhibition (Fig. 1B). Many previously reported substrates, including the aforementioned substrates and NFE2L2, DEPTOR, and CDC25A, were detected only after MG132 treatment. In fact, the levels of 32 proteins demonstrated a median 2-fold or greater increase following MG132 treatment, compared to two proteins and the mitoribosome, whose levels decreased after treatment. Based on these experiments, putative novel substrates included APC, MTSS1L, TFAP4, RASSF3, MAST3, and AEBP2.

FBXW11 and BTRC bind a short amino acid motif in substrate proteins referred to as a degron. Focused study of many known substrates has defined the consensus degron to be DSGXXS. To identify degron-containing proteins, including degron variants, within the FBXW11 and BTRC interaction networks, we used the GLAM2 algorithm and the sequence of known substrates to probabilistically reveal position-specific preferences within the degron (Fig. 1C). This revealed that 65 of 151 FBXW11 interacting proteins contained a statistically defined degron sequence (shown as orange nodes within Fig. 1). Importantly, these proteins demonstrated a statistically significant increase in the response to MG132 compared to degron-deficient FBXW11 interacting proteins (two-tailed t test with unequal variance, $P = 0.034$). We validated several of the FBXW11 protein interactions, including those whose interactions were stabilized by MG132 treatment. Streptavidin affinity purification of SBPCBPHA-FBXW11 and Western blot analysis confirmed associations with DOCK1, NUDC, DAP3, and USP47. MG132-induced interactions with STK3/STK4 and TBC1D4 were also confirmed (Fig. 1D). As a control, we confirmed that SBPCBPHA-tagged-CTNNB1^{SA}, which does not bind FBXW11 or BTRC, did not cocomplex with the analyzed proteins.

RAPGEF2 is an FBXW11 substrate. Among the FBXW11 interacting proteins that contained a predicted degron and responded to MG132 treatment, we selected RAPGEF2 for further validation and functional study. We first validated the protein-protein interactions by immunoprecipitation-Western blot analysis, RAPGEF2 PAC-based proteomics, and subcellular colocalization studies. Western blot analysis of immunopurified FLAG-tagged FBXW11 revealed an MG132-induced association with endogenous RAPGEF2. Importantly, this short treatment did not result in an increase in total cellular levels of RAPGEF2 (Fig. 2A). Reciprocally, endogenous BTRC was detected in protein complexes isolated by immunopurification of ectopically expressed FLAG-RAPGEF2 following MG132 treatment; antibodies which recognize endogenous FBXW11 are not available (Fig. 2B). In agreement, we found that overexpressed RAPGEF2 was immunoprecipitated with both BTRC and FBXW11 after MG132 treatment (Fig. 2C).

Next, we defined the RAPGEF2 protein interaction network by FLAG-based immunoprecipitation and mass spectrometry (IPMS) before and after a 2-h MG132 treatment (Fig. 2D). The MAGI1 and MAGI3 proteins, which are known RAPGEF2 interacting proteins, were detected irrespective of the presence or absence of MG132 treatment. Novel putative interacting proteins, including TJP1 (ZO1/2), PTPN13, TNKS, and EPB41L5, were also discovered. In agreement with the FBXW11 APMS profiling, MG132 treatment resulted in a greater than 5-fold increase in the FBXW11 level within the RAPGEF2 protein complex (Fig. 2E). Finally, to complement the biochemistry, we determined the subcellular distribution of RAPGEF2, BTRC, and FBXW11 in HEK293 cells by epifluorescence microscopy (Fig. 2F). When expressed alone, YFP-RAPGEF2 exhibited a cytosolic distribution with apparent enrichment on centrosomes, proximal to nuclei (Fig. 2F, arrowhead). Indeed, immunofluorescence staining of HEK293 transfected with YFP-RAPGEF2 using antibodies against γ-tubulin confirmed localization of RAPGEF2 to centrosomes (data not shown). FLAG-BTRC was mainly nuclear, while FLAG-FBXW11 exhibited a predominantly cytosolic distribution (Fig. 2F). Interestingly, and consistent with physical association, coexpression of YFP-RAPGEF2 with either FLAG-BTRC or FLAG-FBXW11 resulted in subcellular redistribution of the protein complex (Fig. 2G). Coexpressed FLAG-BTRC and YFP-RAPGEF2 colocalized in numerous cytoplasmic puncta, while coexpressed FLAG-FBXW11 and YFP-RAPGEF2 colocalized in large cytoplasmic aggregates and, to a lesser extent, at the plasma membrane (Fig. 2G, arrowhead and arrow, respectively). Confocal images of HEK293 cells coexpressing FLAG-FBXW11 and YFP-RAPGEF2 further confirmed colocalization of these proteins and localized the large aggregate to perinuclear space (Fig. 2H). Together, the PAC analysis, focused biochemistry, and cell localization studies confirm RAPGEF2 to be a MG132-induced FBXW11 and BTRC interacting protein.

FBXW11 regulates RAPGEF2 protein stability. We next tested whether FBXW11 and BTRC regulate RAPGEF2 protein stability. First, RAPGEF2 protein levels increased following treatment with MG132 proteasome inhibitor, implying that RAPGEF2 protein is regulated by proteasome-mediated degradation (Fig. 3A). Second, ectopic FBXW11 expression resulted in decreased steady-state levels of coexpressed RAPGEF2 (Fig. 3B). Conversely, concurrent siRNA-mediated silencing of both FBXW11 and BTRC strongly increased the level of RAPGEF2 protein expression. This increase was detected by Western blotting and fluorescence microscopy (Fig. 3C and D, respectively). The NEDD4 ubiquitin ligase was previously reported to negatively regulate RAPGEF2 protein stability (40). Compared to FBXW11/BTRC

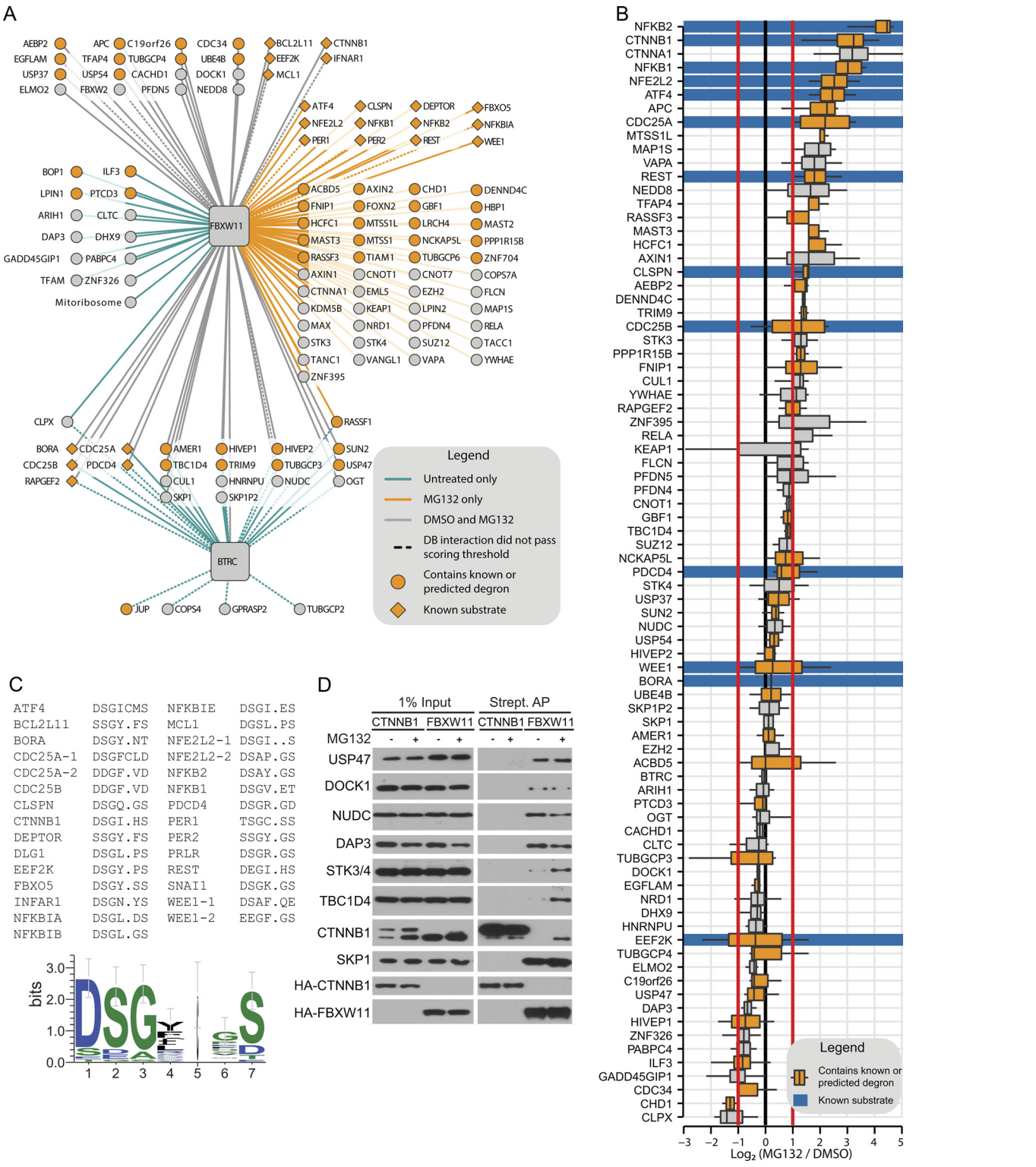

FIG 1 Substrate trapping proteomic analysis of FBXW11. (A) Annotated protein-protein interaction network for FBXW11 and BTRC in HEK293T cells. High-confidence interactions are shown and were defined by the CompPASS scoring algorithm. Previously reported interactions that did not pass the CompPASS threshold are noted with a dashed edge. Protein interactions were defined for FBXW11 in the absence and presence of MG132 (10 μM, 2 h). Complete unfiltered data are provided in Table S1 in the supplemental material. DB, database. (B) Spectral count ratios of FBXW11 interacting proteins after treatment with MG132 or DMSO followed by either FLAG-FBXW11 or TAP-FBXW11 APMS. Box plots are representative of the results of four pairs of replicate biological experiments. (C) Multiple-sequence alignment of published BTRC and FBXW11 substrate degrons. (D) HEK293T cells stably expressing SBPHA-CTNNB1^{SA} or SBPHA-FBXW11 were treated with 10 μM MG132 for 2 h before lysis and streptavidin affinity purification (Strept. AP). Associated endogenous proteins were detected by immunoblot analysis.

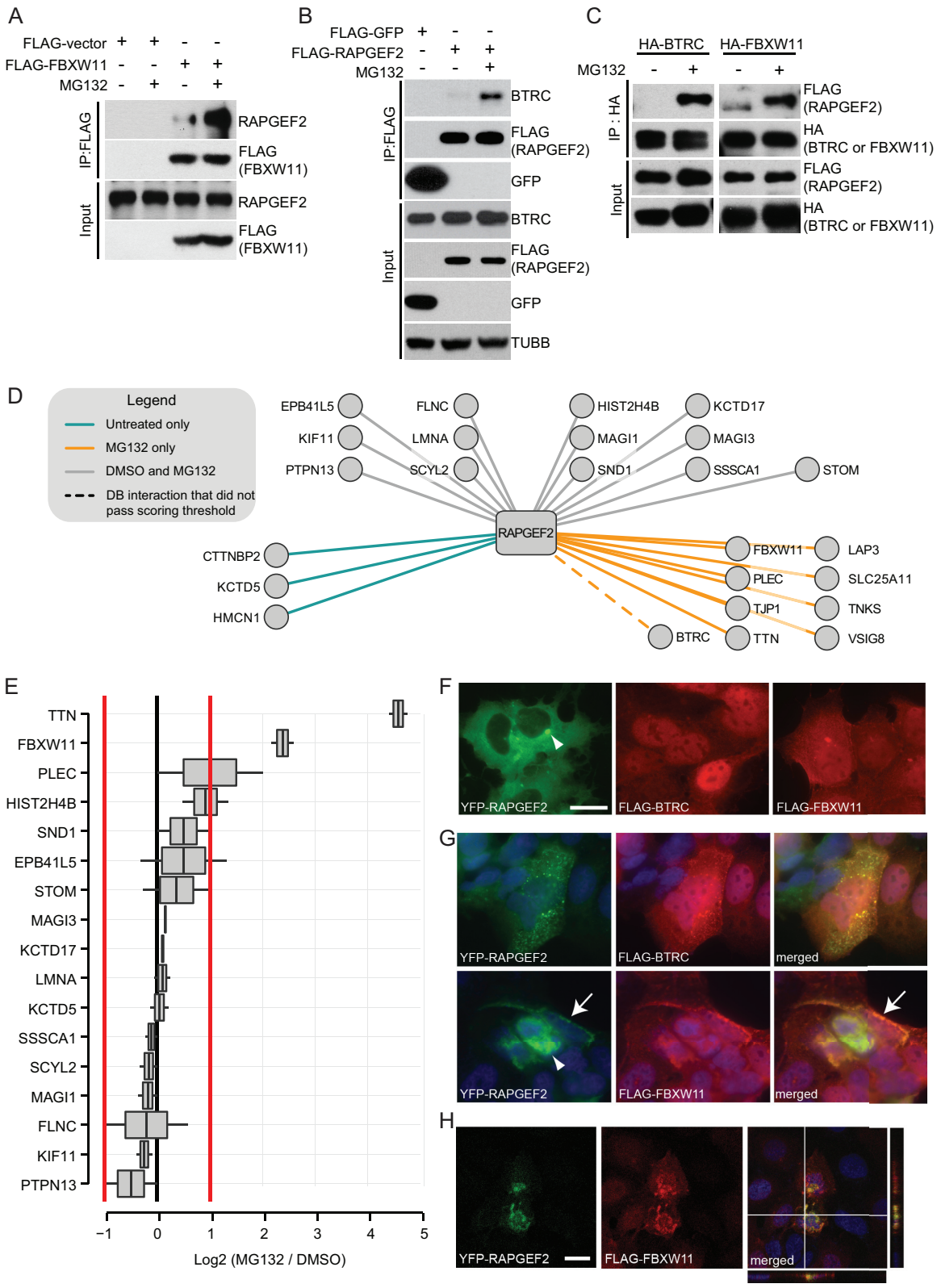

FIG 2 Proteasome inhibition increases the abundance of RAPGEF2 within FBXW11 and BTRC protein complexes. (A and B) Western blot analysis of FLAG-FBXW11 (A) or FLAG-RAPGEF2 (B) immunopurified protein complexes before and after a 2-h MG132 treatment. TUBB, β-tubulin. (C) HEK293 cells were cotransfected with plasmids expressing FLAG-RAPGEF2 and HA-BTRC or HA-FBXW11, followed by treatment with DMSO or MG132 for 2 h. Cell lysates or anti-HA immunoprecipitates were subjected to immunoblot analysis with the indicated antibodies. (D) HEK293T cells expressing FLAG-RAPGEF2 were treated with MG132 for 2 h before lysis, FLAG immunoprecipitation, and mass spectrometry analysis. High-confidence protein interactions are shown, and data indicate the dependency on MG132 treatment. (E) Spectral count ratios of RAPGEF2 interacting proteins (MG132/DMSO). (F) HEK293 cells transfected with

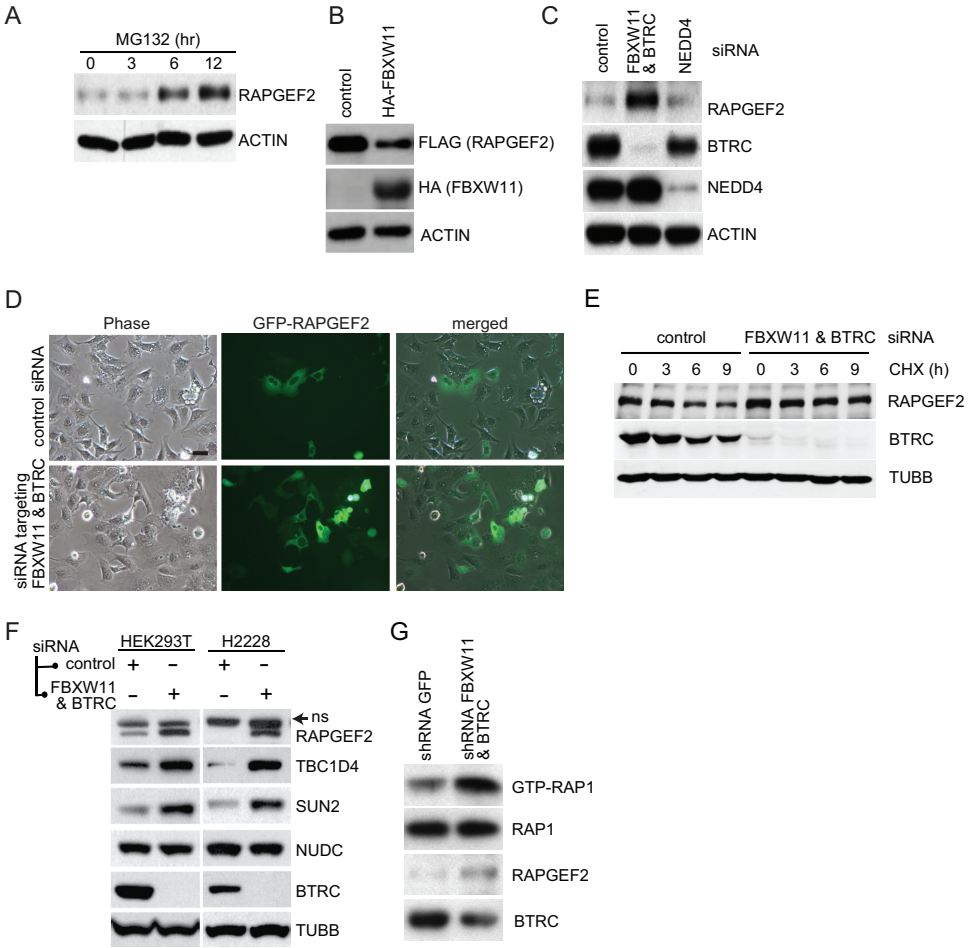

FIG 3 RAPGEF2 is regulated by FBXW11/BTRC-mediated protein degradation. (A) Western blot analysis of HEK293 cells treated with 10 μM MG132 for the indicated periods of time. (B) Western blot analysis of HEK293 cells overexpressing FLAG-RAPGEF2 with or without overexpression of HA-FBXW11. (C) Western blot analysis of HEK293 cells transfected with the indicated siRNAs. (D) HEK293 cells cotransfected with the indicated siRNAs and YFP-RAPGEF2 were fixed 72 h posttransfection and analyzed by phase contrast and epifluorescence microscopy. Scale bar, 40 μm. (E) HEK293 cells were transfected with control and FBXW11/BTRC siRNAs and treated with 40 μg/ml cycloheximide (CHX) for the indicated times. Cell lysates were subjected to immunoblot analysis with anti-RAPGEF2, anti-BTRC, or anti-β-tubulin (TUBB) antibodies. (F) Control siRNAs or siRNAs cotargeting BTRC and FBXW11 were transfected into HEK293 and H2228 cells for 48 h. Cell lysates were subjected to immunoblot analysis with the indicated antibodies. ns, nonspecific. (G) Cell lysates from HEK293 cells stably expressing shRNA against GFP or BTRC and FBXW11 were assessed by pulldown analysis with GST-RalGDS RAP-binding domain (RBD), and the pulldown proteins were then immunoblotted with anti-RAP1 antibody to measure the levels of active GTP-RAP1.

silencing, siRNA-mediated suppression of NEDD4 did not affect RAPGEF2 protein levels (Fig. 3C). Third, the half-live of endogenous RAPGEF2 was increased in cells depleted of FBXW11/BTRC relative to control siRNA transfected cells (Fig. 3E). Fourth, FBXW11/BTRC control over RAPGEF2 protein levels was observed in H2228 lung adenocarcinoma cells (Fig. 3F). In addition to RAPGEF2, we also observed an increase in TBC1D4 and SUN2 levels following depletion of FBXW11/BTRC in both HEK293 and H2228 cell lines, which supports the spectral ratios detected by PAC-based analysis (Fig. 1B). Finally, we used small hairpin RNA (shRNA) vectors to stably cosuppress FBXW11 and BTRC in HEK293T cells. These cells express increased levels of RAPGEF2 and concordantly increased levels of GTP-bound RAP1, a RAPGEF2 substrate (Fig. 3G). Together, these data establish that FBXW11/BTRC negatively regulates RAPGEF2 protein stability and activity.

FBXW11 ubiquitinates RAPGEF2. To test whether FBXW11 or BTRC ubiquitinates RAPGEF2, we performed immunoprecipitation and Western blot analyses under denaturing conditions. siRNA-mediated silencing of FBXW11 or BTRC resulted in strong

YFP-RAPGEF2 (green), FLAG-BTRC, or FLAG-FBXW11 were fixed, stained for FLAG (red), and analyzed using epifluorescence microscopy. (G) HEK293 cells were cotransfected with YFP-RAPGEF2 (green) and FLAG-BTRC or with YFP-RAPGEF2 (green) and FLAG-FBXW11, fixed, stained for FLAG (red), and analyzed using epifluorescence microscopy. Note the large RAPGEF2 aggregate (arrowhead) and the localization of RAPGEF2 at the plasma membrane (arrow) when coexpressed with FBXW11. (H) HEK293 cells cotransfected with YFP-RAPGEF2 (green) and FLAG-FBXW11 were fixed, stained for FLAG (red), and analyzed by confocal microscopy. A single Z-slice is shown; orthogonal images are shown in vertical and horizontal boxes for the merged image. All imaging studies were analyzed in two independent experiments imaged on two different days. DAPI was used to stain DNA. Scale bars, 20 μm.

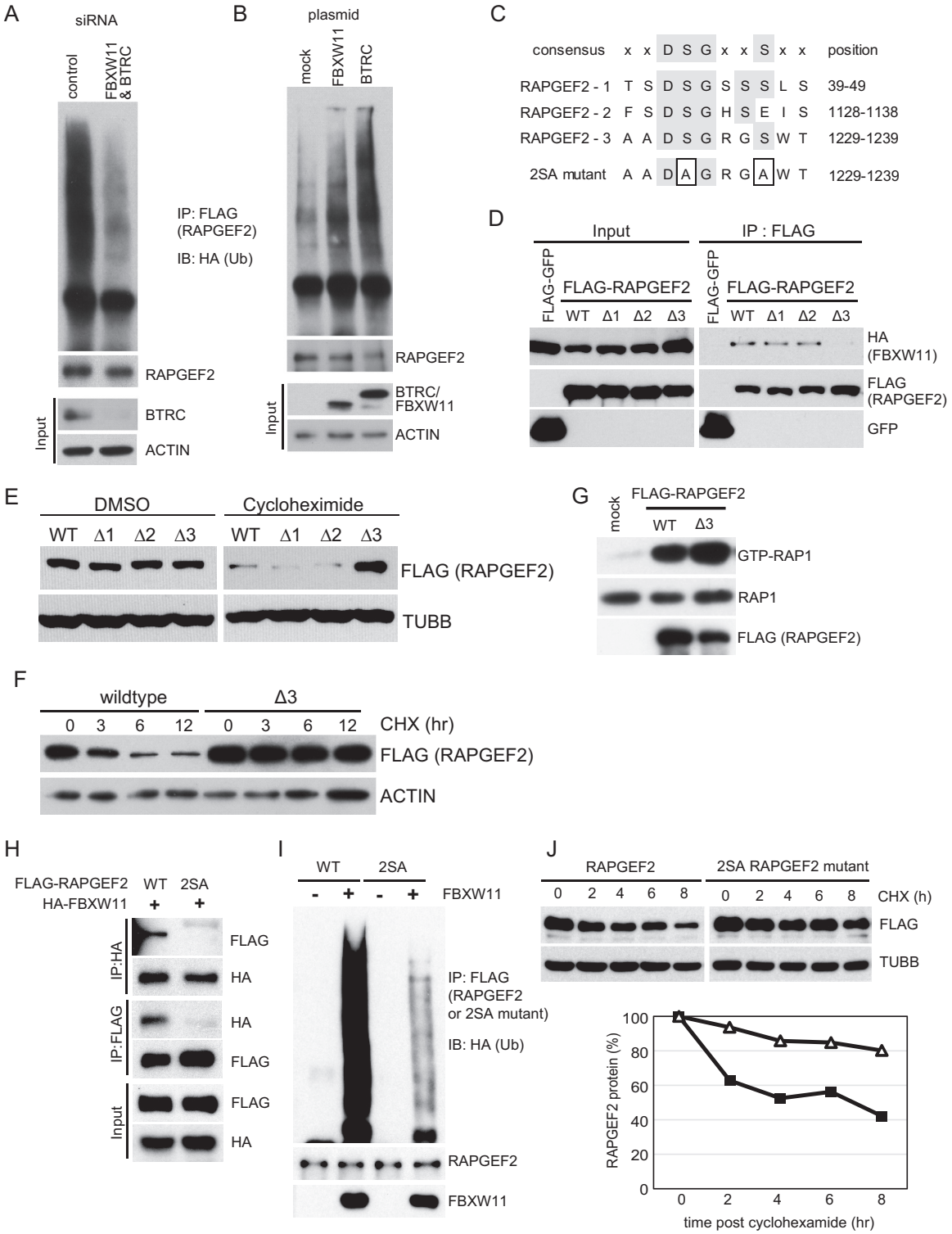

FIG 4 Identification of a degron motif within RAPGEF2 that is required for FBXW11 binding and ubiquitylation. (A) HEK293 cells were transfected with control siRNAs or siRNAs cotargeting BTRC and FBXW11 for 24 h, followed by transfection with HA-ubiquitin (Ub) and FLAG-RAPGEF2 for 48 h. Cells were then treated with MG132 for 6 h before immunoprecipitation and immunoblot analysis. (B) HEK293 cells were cotransfected with plasmids expressing FLAG-RAPGEF2, HA-ubiquitin, and HA-BTRC or HA-FBXW11 for 48 h, followed by treatment with 10 μM MG132 for 6 h. Immunoprecipitated FLAG-RAPGEF2 complexes were subjected to immunoblot analysis. (C) Amino acid sequence alignment of three degron motifs found within RAPGEF2. The sequence of an alanine mutant motif 3 protein is shown at the bottom of the panel as 2SA. (D) RAPGEF2 degron motifs were individually deleted to yield the Δ constructs. These were coexpressed with HA-FBXW11 in HEK293T cells before lysis, FLAG-IP, and immunoblot analysis for the indicated proteins. (E) HEK293 cells were transfected with the indicated FLAG-tagged plasmids for 48 h followed by an 8-h CHX treatment. Cell lysates were subjected to immunoblot analysis with anti-FLAG or anti-β-tubulin antibodies. (F) HEK293 cells were transfected with plasmids expressing the FLAG-tagged wild type or a Δ3 (deletion of the third

suppression of RAPGEF2 ubiquitylation, and overexpression of either BTRC or FBXW11 increased RAPGEF2 ubiquitylation (Fig. 4A and B, respectively). The RAPGEF2 protein contains three putative FBXW11/BTRC recognition domains, or degrons (Fig. 4C). To determine which degron motif mediates FBXW11/BTRC binding, three internal deletion mutants of RAPGEF2 were constructed and evaluated by immunoprecipitation and Western blot analysis. The RAPGEF2-Δ3 mutant, in which the third potential degron motif was deleted, failed to bind to HA-tagged FBXW11 (Fig. 4D). Compared to wild-type protein, the RAPGEF2-Δ3 mutant was considerably more stable after cycloheximide (CHX) treatment and resulted in greater GTP loading of RAP1 (Fig. 4E to G). To further validate and extend these data, we generated a mutant in which two serine-to-alanine substitutions were introduced (2SA) (Fig. 4C). RAPGEF2-2SA, like RAPGEF2-Δ3, failed to cocomplex with FBXW11 (Fig. 4H). RAPGEF2-2SA also demonstrated reduced levels of ubiquitylation and concordantly increased protein stability compared to wild-type RAPGEF2 (Fig. 4I and J, respectively). Taken together, these results suggest that the third degron motif in RAPGEF2 mediates FBXW11 binding and ubiquitylation.

RAPGEF2 promotes multinucleation. While performing subcellular localization studies of ectopically expressed RAPGEF2 in HEK293 cells, we observed striking changes in nuclear morphology (Fig. 5A, arrow). Specifically, RAPGEF2 overexpression resulted in nuclear multilobulation (multiple lobes per nucleus) and multinucleation (cells containing multiple distinct nuclei). In addition, a distinct subset of YFP-RAPGEF2-positive cells demonstrated multinucleation, as evidenced by DAPI staining (Fig. 5A, arrowheads). To quantitatively determine whether expression of RAPGEF2 could induce the generation of multinucleated and nuclear multilobulated cells, we transiently expressed YFP-RAPGEF2 and quantified the percentage of YFP-RAPGEF2-positive cells containing 1, 2, 3, 4, or more nuclei, or a multilobulated nucleus, at 24, 48, and 72 h posttransfection in lamin B immunostaining preparations. As seen in Fig. 5B, the percentage of multinucleated cells at 24 h posttransfection was higher among cells expressing YFP-RAPGEF2 (~13%) than among control GFP-expressing cells (1.86%). Moreover, nuclear multilobulation was found only in cells expressing YFP-RAPGEF2 (~2.90%). The percentages of both multinucleation and nuclear multilobulation showed further increases at 48 h posttransfection in cells expressing YFP-RAPGEF2 (~22% and 12.5%, respectively) but did not increase to the same extent in control cells (~3.5% and 0%, respectively). At 72 h posttransfection, the percentages of multinucleation and nuclear multilobulation were decreased in cells expressing YFP-RAPGEF2 compared to cells expressing YFP-RAPGEF2 at 48 h posttransfection. Despite these decreases, the percentage of multinucleation at 72 h posttransfection was pronouncedly higher in cells expressing YFP-RAPGEF2 than in control cells.

To further validate these phenotypes, we isolated a clonal population of HEK293 cells stably expressing YFP-RAPGEF2. In agreement with the transient-transfection experiments, cells stably expressing YFP-RAGEF2 displayed increased multinucleation compared to parental HEK293 cells (Fig. 5C and D). Interestingly, the nuclear multilobulation observed in transient analyses was not observed in either parental HEK293 cells or HEK293 cells stably expressing YFP-RAPGEF2 (Fig. 5C and D).

Next, we tested whether RAPGEF2 overexpression resulted in an increased DNA ploidy, as measured by DNA content analyses, by flow cytometry. For this, HEK293 cells transiently transfected with GFP or YFP-RAPGEF2 were stained with propidium iodide 48 h posttransfection. Overexpression of RAPGEF2 did not significantly affect cell cycle distributions. Consistent with the multinucleation observed in our morphological analysis, RAPGEF2 expression increased the level of DNA content relative to control transfected cell results (Fig. 5E). We also tested whether RAPGEF2 silencing impacted nuclear number or morphology. We found that RAPGEF2 depletion by siRNA had no effect on the percentage of multinucleated cells and that no cells depleted of RAPGEF2 exhibited nuclear multilobulation (Fig. 5F and G). Moreover, RAPGEF2 depletion had no effect on the cell cycle distribution or the percentage of cells exhibiting DNA content greater than 4 N (Fig. 5H). Altogether, these findings suggest that elevated expression of RAPGEF2 induces cell multinucleation.

RAPGEF2-induced multinucleation is independent of GEF and RAP1 activities. To determine whether RAPGEF2-induced multinucleation was dependent upon the RAPGEF catalytic activity, we generated a GEF-dead RAPGEF2 mutant. To accomplish this, we modeled the primary sequence of the CDC25 homology domain on the structure of the CDC25 homology domain of another RAPGEF, EPAC2, bound to RAP1 (RCSB database identifier 3CF6) (41). This model predicted residues within RAPGEF2 that mediate interaction with RAP1 (Fig. 6A and B). Mutant RAPGEF2 harboring the triple mutation K875A/F879A/N884A was constructed by site-directed mutagenesis, and its lack of GTP exchange activity for RAP1 was confirmed by performing a RAP pulldown assay (Fig. 6C). Unexpectedly, when overexpressed in HEK293 cells, the GEF-dead RAPGEF2 mutant retained its ability to promote both multinucleation and nuclear multilobulation (Fig. 6D). Consistent with this, DNA content analysis demonstrated an increase in the percentage of cells exhibiting DNA content greater than 4 N in populations expressing the dead-RAPGEF2 mutant (Fig. 6E). To confirm these results, HEK293 cells were transfected with constitutively active or dominant-negative RAP1A and RAP1B (RAP1A/B) (RAP1-CA and RAP1-DN, respectively) before quantitation of multinucleated cells; RAP1-CA and RAP1-DN overexpression impacted neither the number nor the shape of nuclei (Fig. 6D). These results support the idea of a GEF- and RAP1-independent function for RAPGEF2 in controlling multinucleation.

DSG motif) mutant of RAPGEF2 for 48 h followed by treatment with 40 μg/ml CHX for the indicated time. Cell lysates were subjected to immunoblot analysis with anti-FLAG or actin antibodies. (G) HEK293T cells were transfected with the indicated RAPGEF2 plasmid before lysis and assessment by pulldown analysis with GST-RalGDS(RBD). The bound proteins were then were immunoblotted with anti-RAP1 antibody to measure the active GTP-RAP1 levels. (H) Two serine residues in the third DSGXXS motif of RAPGEF2 were substituted with alanine to obtain the RAPGEF2 mutant (2SA). This mutant was transfected with HA-FBXW11 into HEK293 cells, followed by treatment with 10 μM MG132 for 2 h. Cell lysates or anti-HA immunoprecipitates were subjected to immunoblot analysis with the indicated antibodies. (I) HEK293 cells were cotransfected with plasmids expressing HA-ubiquitin, FBXW11, and the FLAG-tagged wild type or a 2SA mutant of RAPGEF2 for 48 h, followed by treatment with 10 μM MG132 for 6 h. Equal amounts of anti-FLAG immunoprecipitates were subjected to immunoblot analysis (IB) with anti-HA antibodies. (J) Western blot analysis of HEK293 cells expressing the FLAG-tagged wild type or a 2SA mutant of RAPGEF2 after 40 μg/ml CHX treatment for the indicated times.

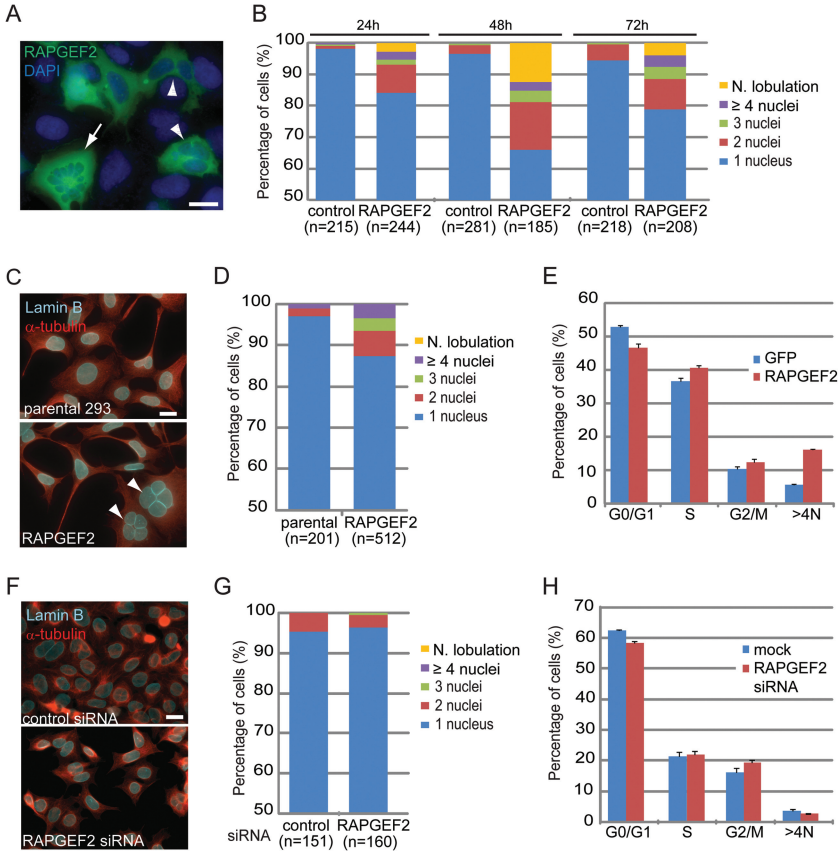

FIG 5 RAPGEF2 induces multinucleation in a GEF- and Rap1-activity-independent fashion. (A) HEK293 cells transiently expressing YFP-RAPGEF2 were fixed and imaged using epifluorescence microscopy. DAPI was used for DNA labeling. Note the presence of nuclear multilobulated (arrow) and multinucleated (arrowhead) cells. (B) Quantification of multinucleation and nuclear multilobulation. HEK293 cells transfected with HcRed (control) or RAPGEF2 were scored based on number of nuclei and nuclear lobulation at 24 h and 48 h posttransfection. n, number of cells scored. (C) Parental HEK293 cells and cells stably expressing YFP-RAPGEF2 were fixed, stained for lamin B (cyan) and tubulin (red), and imaged using epifluorescence microscopy. Note the presence of multinucleated cells (arrowheads). (D) Quantification of multinucleation and nuclear multilobulation in parental HEK293 cells and cells stably expressing YFP-RAPGEF2. (E) Cell cycle distribution analyses by flow cytometry of parental HEK293 cells and HEK293 cells transfected with GFP or WT-RAPGEF2 stained with propidium iodide. Data are shown as means ± standard errors of the means (SEM) of the results of triplicate biological experiments. (F) HEK293 cells transfected with the indicated siRNAs and stained for lamin B (cyan) and tubulin (red). (G) Quantification of multinucleation and nuclear multilobulation in the cells whose results are shown in panel F. Data are representative of the results of three independent replicate biological experiments. (H) Cell cycle distribution analyses by flow cytometry of mock-transfected HEK293 cells or HEK293 cells transfected with RAPGEF2 siRNAs and stained with propidium iodide. Data are shown as means ± SEM of the results of triplicate biological experiments. Scale bars, 20 μm.

Multinucleation can result from several distinct processes, including cytokinesis failure, cell-cell fusion, centrosome overduplication, and endoreplication (42, 43). To further delineate the cellular mechanism(s) by which RAPGEF2 promotes multinucleation, we performed time-lapse microscopy of HEK293 cells transiently expressing YFP-RAPGEF2 alone or in combination with cherry-NLS. Both experiments revealed that RAPGEF2 overexpression promoted cell-cell fusion events, and, perhaps surprisingly, alterations in cytokinesis were not observed (Fig. 6F; see also Videos S1 and S2 in the supplemental material). These data suggest that RAPGEF2 promotes the generation of multinucleated cells by inducing cell-cell fusion.

DISCUSSION

In general, the phenotypic importance of an E3 ubiquitin ligase complex can be inferred from the function of its substrates and the nature of ubiquitin chain linkage. Until recently, comprehensive substrate identification has been challenging. Several experimental approaches now provide generally applicable and unbiased technologies for medium-throughput substrate identification. These approaches, including their relative strengths and weaknesses, have been recently reviewed by Harper and Tan (8). The parallel adaptor capture proteomics (PAC) method uses comparative mass spectrometry analysis of immunopurified ubiquitin ligase adapter proteins to identify putative substrates. Proteins which increase in abundance within the purified E3 complex after proteasome or NEDD8 inhibition constitute candidate substrates and substrate-associated proteins. The PAC-based method was used to study 23 unique E3 adapter proteins, including 21 leucine-rich repeat FBXL proteins (13). Of 27 putative new substrates identified, 13 demonstrated increased protein levels following NEDD8 inhibition, supporting the idea of ubiquitin-dependent turnover. Here, we used PAC-based proteomics to study the FBXW11 ubiquitin ligase adapter protein. We discovered 96 interacting proteins, 23 of which demonstrated increased association after proteasome inhibition. These new putative substrates

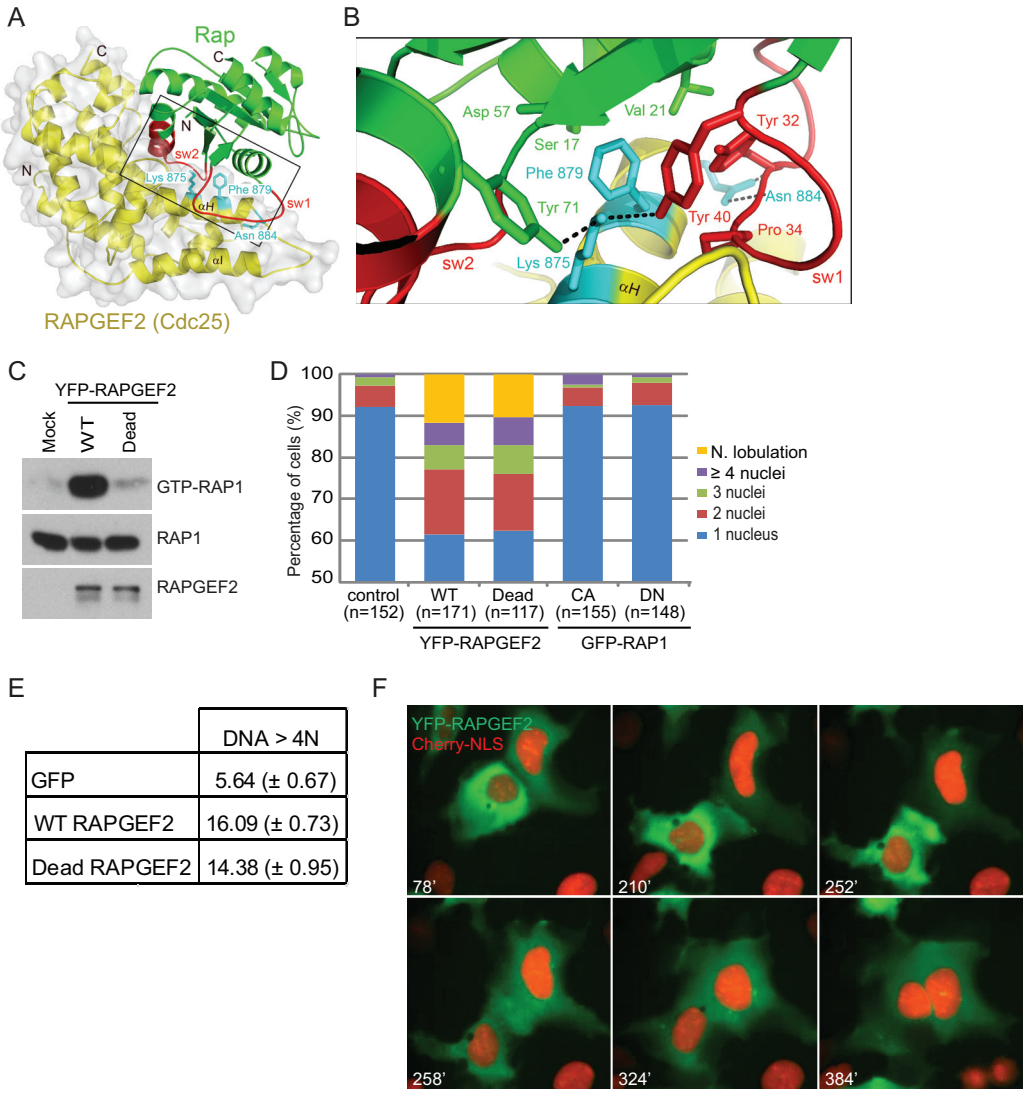

FIG 6 RAPGEF2-induced multinucleation is GEF and Rap1 activity independent. (A) Homology model of RAPGEF2·RAP1. (Left) The Cdc25 domain of RAPGEF2 was modeled using the protein homology/analogy recognition engine 2 (Phyre2) server (71) and superimposed on the structure of EPAC2·RAP1 (41) using Coot (72). The Cdc25 domain of RAPGEF2 is shown as a yellow ribbon, while $Mg2^{+}$/nucleotide-free RAP1 is depicted in green with nucleotide-dependent switches (sw1 and sw2) colored red. Residues Lys 875, Phe 879, and Asn 884 (cyan) within the "helical hairpin" (αH and αI) (73, 74) of the Cdc25 domain of RAPGEF2 are essential for interactions with bound RAP1 and GEF-catalyzed exchange. (B) An expanded view of the boxed area (left) highlights the multiple polar and hydrophobic interactions between residues in the helical hairpin and RAP1. Dashed lines indicate hydrogen bonding. (C) RAP1 pulldown assay with HEK293 cells that were mock transfected or transfected with the wild type or the dead-RAPGEF2 mutant by using GST-RalGDS-RBD beads. (D) Quantification of multinucleation and multilobulation in HEK293 cells transiently expressing HcRed (control), RAPGEF2-WT, RAPGEF2-GEF-dead, constitutively active RAP1 (RAP1 CA), or dominant-negative RAP1 (RAP1 DN). Data are representative of the results of two independent replicate biological experiments. (E) Percentages of cells exhibiting DNA content greater than 4 N. HEK293 cells were transfected with GFP or wild-type or GEF-dead RAPGEF2, stained with propidium iodide, and analyzed by flow cytometry. Data are shown as mean percentages ± SEM of the results of triplicate biological experiments. (F) Time-lapse images of HEK293 cells cotransfected with cherry-nuclear localization signal (Cherry-NLS) and YFP-RAPGEF2. Cells were imaged for 19 h at 6-min intervals.

include TBC1D4, SUN2, STK3, and the recently reported RAPGEF2 protein (28).

Taken together, our results further support the power of PAC-based proteomics for E3 substrate identification. That said, PAC data sets must be interpreted wisely. First, an appreciation of the high false-discovery rates common to IPMS studies is needed; probabilistic scoring algorithms for IPMS data sets are conveniently provided by SAINT, HGScore, and CompPASS (39, 44, 45). Second, PAC-based interaction networks and identified candidate substrates are not comprehensive. Monoubiquitylated substrates and those not degraded by the proteasome are unlikely to experience enrichment within PAC-based analyses. For example, we did not identify the lysosomal targeted SCF^{FBXW11} substrates IFNAR1 and PRLR within our studies (46, 47). Last, the relative abundances and kinetics of substrate turnover must be considered; a low-abundance substrate with a low rate of ubiquitylation and/or degradation does not experience enrichment to the same degree as rapidly catalyzed substrates. Time course studies would prove informative. By extension, whereas most substrates exhibit relative increases within the E3 complex, low-affinity pseudosub-

strates, for example, HNRNPU, may show no change or a decrease within the complex (48).

Several of the putative substrates we identified have not previously been associated with ubiquitylation, regulated protein stability, or the SCF^{FBXW11} complex. *TBC1D4* encodes a GAP for the small GTPase Rab that controls insulin-dependent trafficking of the GLUT4 glucose transporter in skeletal muscle cells and in adipocytes (49, 50). Upon insulin stimulation, AKT induces phosphorylation of TBC1D4 at multiple sites, inactivating its GAP activity, which in turn prevents translocation of GLUT4 from intracellular storage vesicles to the cell surface (51, 52). The importance of *TBC1D4* in human disease was recently illustrated though genetic association studies of a Greenlandic population experiencing a rapidly increasing incidence of type 2 diabetes (53). That study revealed a homozygous truncating variant in *TBC1D4* in 17% of the population; allele carriers, even in the heterozygous state, demonstrated impaired glucose homeostasis. Our data suggest a new mechanism by which TBC1D4 activity might be regulated and an additional link between FBXW11 and glucose homeostasis. It was also recently reported that SCF^{FBXW11} negatively regulates the stability of ELAV1 and PFKFB3, both of which regulate glycolysis and energy homeostasis (54, 55).

SUN2, together with SUN1, localizes at the inner nuclear membrane (56, 57), and both proteins interact with lamin proteins at the inner nuclear membrane and recruit KASH proteins to the outer nuclear membrane, playing an important role in proper positioning of the nucleus in cells (58) and in the DNA damage response (59), as well as contributing to the progression of laminopathies (60). Of note, it was recently suggested that SUN proteins are accumulated in cells that express lamin A mutations, leading to cellular toxicity mediated by Golgi disruption and hyperactive DNA damage response (61). Therefore, it is possible that the increased stability of SUN proteins in lamin A-defective cells is attributable to SCF^{FBXW11}-mediated protein stability regulation.

We focused our biochemical and functional studies on RAPGEF2, a guanine exchange factor (GEF) for the RAP1/2 small GTPases. While we were preparing this paper for publication, Magliozzi et al. reported the ubiquitylation of RAPGEF2 by SCF^{FBXW11} and SCF^{BTRC} (28). RAPGEF2 ubiquitylation and subsequent degradation required priming phosphorylation by IκB kinase beta (IKKβ) and CK1α and was triggered by promigratory signals. Expression of degron mutant RAPGEF2 led to increased RAP1 activity and suppression of cell migration. Our findings, including the identification of the degron motif and the activation of RAP1 activity following FBXW11 silencing, strongly agree with those reported by Magliozzi et al. However, in contrast to their findings, we found that preventing FBXW11-mediated RAPGEF2 degradation caused RAP1- and GEF-independent promotion of cell fusion and multinucleation.

Consistent with their physical interaction, we found that expression of RAPGEF2 affected the subcellular localization of BTRC and FBXW11 and, reciprocally, that expression of BTRC and FBXW11 affected RAPGEF2 localization. RAPGEF2 localizes to sites of cell-cell contact, partially colocalizing with CTNNB1 and TJP1 (62). RAPGEF2 also physically interacts with the MAGI proteins, which in turn bind CTNNB1 at cell-cell contacts to recruit RAP1 (63). Our observation that RAPGEF2 is mainly diffusely cytosolic when expressed alone under subconfluent conditions but colocalizes with FBXW11 at the plasma membrane sites may support the idea of a role for RAPGEF2 as a scaffold protein. Specifically, RAPGEF2 may carry or recruit FBXW11 to the cell cortex, where it impacts the ubiquitylation of a distinct pool of binding partners. In this context, we hypothesize that the RAPGEF2-FBXW11 complex and possibly associated proteins respond to cell confluence and contribute to downstream signaling pathways. We also detected RAPGEF2 at centrosomes; this was confirmed by colocalization studies performed with gamma-tubulin (data not shown). These results suggest that RAPGEF2 may play different roles, some of which may not require GEF activity, in different subcellular compartments.

The most striking phenotype we observed when interrogating the FBXW11-RAPGEF2 interaction was the appearance of cells with multiple nuclei following RAPGEF2 overexpression. While further study is needed to establish the precise cellular mechanism of multinucleation, our live-cell microscopy experiments revealed that RAPGEF2 overexpression results in cell-cell fusions and surprisingly, does not impact mitosis or cell cycle progression. Given its role and location within membrane-associated protein complexes, it is possible that RAPGEF2 induces changes in cell-cell adhesion properties that result in altered cell permeability and membrane fusion. An important unresolved issue regards the epistatic and phenotypic relationships between BTRC/FBXW11 loss, RAPGEF2 increase, and multinucleation/aneuploidy. In other words, does FBXW11/BTRC loss result in RAPGEF2-dependent multinucleation, and is this mediated by cell-cell fusion? Many studies have shown that FBXW11 and BTRC deficiency results in cell cycle arrest, centrosome duplication, and mitotic spindle dysfunction, owing to failed degradation of various substrates, including EMI1(FBXO5), REST, CDC25A, WEE1, PLK1, and PLK4 (64). Spermatids from BTRC knockout mice display multinucleation (65). Although the experiments are incomplete, our data suggest that loss of function for FBXW11 and BTRC results in rapid cell cycle arrest, centrosome amplification, and multinucleation in a manner independent of cell-cell fusion. It is likely that the altered cell cycle progression masks any effect of FBXW11/BTRC on RAPGEF2-dependent cell-cell fusion. Acute and spatially restricted FBXW11/BTRC inhibition would be required to test this model.

RAPGEF2 is a well-known and physiologically important activator of RAP1 (26, 28, 63, 66). Our data unexpectedly reveal GEF- and RAP-independent functions of RAPGEF2. Specifically, both wild-type RAPGEF2 and GEF-dead RAPGEF2 induced multinucleation and, further, neither dominant-negative nor constitutively active mutants of RAP1 affected multinucleation. To our knowledge, this is the first example of a GEF-independent function for RAPGEF2. Further structure-function analysis of other RAPGEF2 protein domains would provide valuable insight into the underlying mechanics of multinucleation. Additionally, epistatically positioning RAPGEF2-associated proteins such as MAGI1, MAGI3, and PTPN13 with respect to multinucleation and cell fusion is needed.

Cellular multinucleation that arises through cell-cell fusion is a required event for normal development and tissue homeostasis (67). For instance, macrophages undergo fusion leading to the generation of osteoclasts and giant cells, which play fundamental roles in bone absorption and in chronic inflammation, respectively. Likewise, skeletal muscle development occurs through fusion of mononucleated myoblasts (68), while placenta development requires the formation of the trophoblastic syncytium (69). Cell fusion is a genetically programmed process that can be di-

vided into three stages: competence (cell induction and differentiation), commitment (cell determination, migration, and adhesion), and cell fusion (membrane merging and cytoplasmic mixing) (70). Despite its importance and morphological characterization, relatively little is known about the regulatory pathways that control cell-cell fusion. Our current report provides evidence that RAPGEF2 functions in a GEF-independent fashion to mediate cell-cell fusion events.

Based on our data, RAPGEF2 overexpression and multinucleation might be predicted to contribute to the cancer phenotype. Specifically, multinucleated cells likely exhibit increased susceptibility to mitotic/cytokinesis abnormalities which could promote genomic instability. Consistent with this, RAPGEF2 and its interacting protein MAGI-2 were independently identified in an *in vivo* low-copy-number piggyBac insertional mutagenesis screen for drivers of melanoma (27). In that study, transposon mutagenesis (transpogenesis) within the RAPGEF2 locus was predicted to result in an overexpressed full-length protein. In comparison, RAPGEF2 overexpression and subsequent RAP1 activation suppressed invasion and dissemination in breast cancer models (28). Although the idea is speculative, it is possible that RAPGEF2 promotes tumorigenesis early via RAP1-independent cell fusions and represses cancer progression late through RAP1-dependent inhibition of metastasis. Alternatively, RAPGEF2 may differentially impact tumor cell biology depending on the cell type.

ACKNOWLEDGMENTS

This study was supported by grants from the Sidney Kimmel Foundation for Cancer Research (Scholar Award to M.B.M.) and the National Institutes of Health (Director's New Innovator Award to M.B.M., 1-DP2-OD007149-01). R.T.M. is funded by the Howard Hughes Medical Institute.

REFERENCES

1. **Berndsen CE, Wolberger C.** 2014. New insights into ubiquitin E3 ligase mechanism. Nat Struct Mol Biol **21:**301–307. http://dx.doi.org/10.1038/nsmb.2780.
2. **Lydeard JR, Schulman BA, Harper JW.** 2013. Building and remodelling Cullin-RING E3 ubiquitin ligases. EMBO Rep **14:**1050–1061. http://dx.doi.org/10.1038/embor.2013.173.
3. **Grabbe C, Husnjak K, Dikic I.** 2011. The spatial and temporal organization of ubiquitin networks. Nat Rev Mol Cell Biol **12:**295–307. http://dx.doi.org/10.1038/nrm3099.
4. **Hunter T.** 2007. The age of crosstalk: phosphorylation, ubiquitination, and beyond. Mol Cell **28:**730–738. http://dx.doi.org/10.1016/j.molcel.2007.11.019.
5. **Deshaies RJ, Joazeiro CA.** 2009. RING domain E3 ubiquitin ligases. Annu Rev Biochem **78:**399–434. http://dx.doi.org/10.1146/annurev.biochem.78.101807.093809.
6. **Chen T, Zhou T, He B, Yu H, Guo X, Song X, Sha J.** 2014. mUbiSiDa: a comprehensive database for protein ubiquitination sites in mammals. PLoS One **9:**e85744. http://dx.doi.org/10.1371/journal.pone.0085744.
7. **Hornbeck PV, Kornhauser JM, Tkachev S, Zhang B, Skrzypek E, Murray B, Latham V, Sullivan M.** 2012. PhosphoSitePlus: a comprehensive resource for investigating the structure and function of experimentally determined post-translational modifications in man and mouse. Nucleic Acids Res **40:**D261–D270. http://dx.doi.org/10.1093/nar/gkr1122.
8. **Harper JW, Tan MK.** 2012. Understanding cullin-RING E3 biology through proteomics-based substrate identification. Mol Cell Proteomics **11:**1541–1550. http://dx.doi.org/10.1074/mcp.R112.021154.
9. **Arabi A, Ullah K, Branca RM, Johansson J, Bandarra D, Haneklaus M, Fu J, Aries I, Nilsson P, Den Boer ML, Pokrovskaja K, Grander D, Xiao G, Rocha S, Lehtio J, Sangfelt O.** 2012. Proteomic screen reveals Fbw7 as a modulator of the NF-kappaB pathway. Nat Commun **3:**976. http://dx.doi.org/10.1038/ncomms1975.
10. **Peschiaroli A, Dorrello NV, Guardavaccaro D, Venere M, Halazonetis T, Sherman NE, Pagano M.** 2006. SCFbetaTrCP-mediated degradation of Claspin regulates recovery from the DNA replication checkpoint response. Mol Cell **23:**319–329. http://dx.doi.org/10.1016/j.molcel.2006.06.013.
11. **Gao D, Inuzuka H, Tan MK, Fukushima H, Locasale JW, Liu P, Wan L, Zhai B, Chin YR, Shaik S, Lyssiotis CA, Gygi SP, Toker A, Cantley LC, Asara JM, Harper JW, Wei W.** 2011. mTOR drives its own activation via SCF(betaTrCP)-dependent degradation of the mTOR inhibitor DEPTOR. Mol Cell **44:**290–303. http://dx.doi.org/10.1016/j.molcel.2011.08.030.
12. **Liao H, Liu XJ, Blank JL, Bouck DC, Bernard H, Garcia K, Lightcap ES.** 2011. Quantitative proteomic analysis of cellular protein modulation upon inhibition of the NEDD8-activating enzyme by MLN4924. Mol Cell Proteomics **10:**M111.009183. http://dx.doi.org/10.1074/mcp.M111.009183.
13. **Tan MK, Lim HJ, Bennett EJ, Shi Y, Harper JW.** 2013. Parallel SCF adaptor capture proteomics reveals a role for SCFFBXL17 in NRF2 activation via BACH1 repressor turnover. Mol Cell **52:**9–24. http://dx.doi.org/10.1016/j.molcel.2013.08.018.
14. **Yumimoto K, Matsumoto M, Oyamada K, Moroishi T, Nakayama KI.** 2012. Comprehensive identification of substrates for F-box proteins by differential proteomics analysis. J Proteome Res **11:**3175–3185. http://dx.doi.org/10.1021/pr201216u.
15. **Guardavaccaro D, Frescas D, Dorrello NV, Peschiaroli A, Multani AS, Cardozo T, Lasorella A, Iavarone A, Chang S, Hernando E, Pagano M.** 2008. Control of chromosome stability by the beta-TrCP-REST-Mad2 axis. Nature **452:**365–369. http://dx.doi.org/10.1038/nature06641.
16. **Dorrello NV, Peschiaroli A, Guardavaccaro D, Colburn NH, Sherman NE, Pagano M.** 2006. S6K1- and betaTRCP-mediated degradation of PDCD4 promotes protein translation and cell growth. Science **314:**467–471. http://dx.doi.org/10.1126/science.1130276.
17. **Kim W, Bennett EJ, Huttlin EL, Guo A, Li J, Possemato A, Sowa ME, Rad R, Rush J, Comb MJ, Harper JW, Gygi SP.** 2011. Systematic and quantitative assessment of the ubiquitin-modified proteome. Mol Cell **44:**325–340. http://dx.doi.org/10.1016/j.molcel.2011.08.025.
18. **Emanuele MJ, Elia AE, Xu Q, Thoma CR, Izhar L, Leng Y, Guo A, Chen YN, Rush J, Hsu PW, Yen HC, Elledge SJ.** 2011. Global identification of modular cullin-RING ligase substrates. Cell **147:**459–474. http://dx.doi.org/10.1016/j.cell.2011.09.019.
19. **Yen HC, Elledge SJ.** 2008. Identification of SCF ubiquitin ligase substrates by global protein stability profiling. Science **322:**923–929. http://dx.doi.org/10.1126/science.1160462.
20. **Frescas D, Pagano M.** 2008. Deregulated proteolysis by the F-box proteins SKP2 and beta-TrCP: tipping the scales of cancer. Nat Rev Cancer **8:**438–449. http://dx.doi.org/10.1038/nrc2396.
21. **de Rooij J, Boenink NM, van Triest M, Cool RH, Wittinghofer A, Bos JL.** 1999. PDZ-GEF1, a guanine nucleotide exchange factor specific for Rap1 and Rap2. J Biol Chem **274:**38125–38130. http://dx.doi.org/10.1074/jbc.274.53.38125.
22. **Bos JL.** 2005. Linking Rap to cell adhesion. Curr Opin Cell Biol **17:**123–128. http://dx.doi.org/10.1016/j.ceb.2005.02.009.
23. **Bilasy SE, Satoh T, Terashima T, Kataoka T.** 2011. RA-GEF-1 (Rapgef2) is essential for proper development of the midline commissures. Neurosci Res **71:**200–209. http://dx.doi.org/10.1016/j.neures.2011.08.004.
24. **Boettner B, Van Aelst L.** 2007. The Rap GTPase activator Drosophila PDZ-GEF regulates cell shape in epithelial migration and morphogenesis. Mol Cell Biol **27:**7966–7980. http://dx.doi.org/10.1128/MCB.01275-07.
25. **Liao Y, Kariya K, Hu CD, Shibatohge M, Goshima M, Okada T, Watari Y, Gao X, Jin TG, Yamawaki-Kataoka Y, Kataoka T.** 1999. RA-GEF, a novel Rap1A guanine nucleotide exchange factor containing a Ras/Rap1A-associating domain, is conserved between nematode and humans. J Biol Chem **274:**37815–37820. http://dx.doi.org/10.1074/jbc.274.53.37815.
26. **Satyanarayana A, Gudmundsson KO, Chen X, Coppola V, Tessarollo L, Keller JR, Hou SX.** 2010. RapGEF2 is essential for embryonic hematopoiesis but dispensable for adult hematopoiesis. Blood **116:**2921–2931. http://dx.doi.org/10.1182/blood-2010-01-262964.
27. **Ni TK, Landrette SF, Bjornson RD, Bosenberg MW, Xu T.** 2013. Low-copy piggyBac transposon mutagenesis in mice identifies genes driving melanoma. Proc Natl Acad Sci U S A **110:**E3640–E3649. http://dx.doi.org/10.1073/pnas.1314435110.
28. **Magliozzi R, Low TY, Weijts BG, Cheng T, Spanjaard E, Mohammed S, van Veen A, Ovaa H, de Rooij J, Zwartkruis FJ, Bos JL, de Bruin A,**

Heck AJ, Guardavaccaro D. 2013. Control of epithelial cell migration and invasion by the IKKbeta- and CK1alpha-mediated degradation of RAPGEF2. Dev Cell **27:**574–585. http://dx.doi.org/10.1016/j.devcel.2013.10.023.

29. **Emery AC, Eiden MV, Mustafa T, Eiden LE.** 2013. Rapgef2 connects GPCR-mediated cAMP signals to ERK activation in neuronal and endocrine cells. Sci Signal **6:**ra51. http://dx.doi.org/10.1126/scisignal.2003993.
30. **Major MB, Camp ND, Berndt JD, Yi X, Goldenberg SJ, Hubbert C, Biechele TL, Gingras AC, Zheng N, Maccoss MJ, Angers S, Moon RT.** 2007. Wilms tumor suppressor WTX negatively regulates WNT/beta-catenin signaling. Science **316:**1043–1046. http://dx.doi.org/10.1126/science/1141515.
31. **Hast BE, Cloer EW, Goldfarb D, Li H, Siesser PF, Yan F, Walter V, Zheng N, Hayes DN, Major MB.** 9 December 2013, posting date. Cancer-derived mutations in KEAP1 impair NRF2 degradation but not ubiquitination. Cancer Res http://dx.doi.org/10.1158/0008-5472.CAN-13-1655.
32. **Major MB, Roberts BS, Berndt JD, Marine S, Anastas J, Chung N, Ferrer M, Yi X, Stoick-Cooper CL, von Haller PD, Kategaya L, Chien A, Angers S, MacCoss M, Cleary MA, Arthur WT, Moon RT.** 2008. New regulators of Wnt/beta-catenin signaling revealed by integrative molecular screening. Sci Signal **1:**ra12.
33. **Keller A, Nesvizhskii AI, Kolker E, Aebersold R.** 2002. Empirical statistical model to estimate the accuracy of peptide identifications made by MS/MS and database search. Anal Chem **74:**5383–5392. http://dx.doi.org/10.1021/ac025747h.
34. **Vizcaíno JA, Deutsch EW, Wang R, Csordas A, Reisinger F, Rios D, Dianes JA, Sun Z, Farrah T, Bandeira N, Binz PA, Xenarios I, Eisenacher M, Mayer G, Gatto L, Campos A, Chalkley RJ, Kraus HJ, Albar JP, Martinez-Bartolome S, Apweiler R, Omenn GS, Martens L, Jones AR, Hermjakob H.** 2014. ProteomeXchange provides globally coordinated proteomics data submission and dissemination. Nat Biotechnol **32:**223–226. http://dx.doi.org/10.1038/nbt.2839.
35. **Liu G, Zhang J, Larsen B, Stark C, Breitkreutz A, Lin ZY, Breitkreutz BJ, Ding Y, Colwill K, Pasculescu A, Pawson T, Wrana JL, Nesvizhskii AI, Raught B, Tyers M, Gingras AC.** 2010. ProHits: integrated software for mass spectrometry-based interaction proteomics. Nat Biotechnol **28:**1015–1017. http://dx.doi.org/10.1038/nbt1010-1015.
36. **Shannon P, Markiel A, Ozier O, Baliga NS, Wang JT, Ramage D, Amin N, Schwikowski B, Ideker T.** 2003. Cytoscape: a software environment for integrated models of biomolecular interaction networks. Genome Res **13:**2498–2504. http://dx.doi.org/10.1101/gr.1239303.
37. **Frith MC, Saunders NF, Kobe B, Bailey TL.** 2008. Discovering sequence motifs with arbitrary insertions and deletions. PLoS Comput Biol **4:**e1000071. http://dx.doi.org/10.1371/journal.pcbi.1000071.
38. **Franke B, van Triest M, de Bruijn KM, van Willigen G, Nieuwenhuis HK, Negrier C, Akkerman JW, Bos JL.** 2000. Sequential regulation of the small GTPase Rap1 in human platelets. Mol Cell Biol **20:**779–785. http://dx.doi.org/10.1128/MCB.20.3.779-785.2000.
39. **Sowa ME, Bennett EJ, Gygi SP, Harper JW.** 2009. Defining the human deubiquitinating enzyme interaction landscape. Cell **138:**389–403. http://dx.doi.org/10.1016/j.cell.2009.04.042.
40. **Pham N, Rotin D.** 2001. Nedd4 regulates ubiquitination and stability of the guanine-nucleotide exchange factor CNrasGEF. J Biol Chem **276:**46995–47003. http://dx.doi.org/10.1074/jbc.M108373200.
41. **Rehmann H, Arias-Palomo E, Hadders MA, Schwede F, Llorca O, Bos JL.** 2008. Structure of Epac2 in complex with a cyclic AMP analogue and RAP1B. Nature **455:**124–127. http://dx.doi.org/10.1038/nature07187.
42. **Vitale I, Galluzzi L, Senovilla L, Criollo A, Jemaa M, Castedo M, Kroemer G.** 2011. Illicit survival of cancer cells during polyploidization and depolyploidization. Cell Death Differ **18:**1403–1413. http://dx.doi.org/10.1038/cdd.2010.145.
43. **Holland AJ, Cleveland DW.** 2009. Boveri revisited: chromosomal instability, aneuploidy and tumorigenesis. Nat Rev Mol Cell Biol **10:**478–487. http://dx.doi.org/10.1038/nrm2718.
44. **Choi H, Larsen B, Lin ZY, Breitkreutz A, Mellacheruvu D, Fermin D, Qin ZS, Tyers M, Gingras AC, Nesvizhskii AI.** 2011. SAINT: probabilistic scoring of affinity purification-mass spectrometry data. Nat Methods **8:**70–73. http://dx.doi.org/10.1038/nmeth.1541.
45. **Guruharsha KG, Rual JF, Zhai B, Mintseris J, Vaidya P, Vaidya N, Beekman C, Wong C, Rhee DY, Cenaj O, McKillip E, Shah S, Stapleton M, Wan KH, Yu C, Parsa B, Carlson JW, Chen X, Kapadia B, Vijay-Raghavan K, Gygi SP, Celniker SE, Obar RA, Artavanis-Tsakonas S.** 2011. A protein complex network of Drosophila melanogaster. Cell **147:**690–703. http://dx.doi.org/10.1016/j.cell.2011.08.047.
46. **Kumar KG, Krolewski JJ, Fuchs SY.** 2004. Phosphorylation and specific ubiquitin acceptor sites are required for ubiquitination and degradation of the IFNAR1 subunit of type I interferon receptor. J Biol Chem **279:**46614–46620. http://dx.doi.org/10.1074/jbc.M407082200.
47. **Li Y, Kumar KG, Tang W, Spiegelman VS, Fuchs SY.** 2004. Negative regulation of prolactin receptor stability and signaling mediated by SCF-(beta-TrCP) E3 ubiquitin ligase. Mol Cell Biol **24:**4038–4048. http://dx.doi.org/10.1128/MCB.24.9.4038-4048.2004.
48. **Davis M, Hatzubai A, Andersen JS, Ben-Shushan E, Fisher GZ, Yaron A, Bauskin A, Mercurio F, Mann M, Ben-Neriah Y.** 2002. Pseudosubstrate regulation of the SCF(beta-TrCP) ubiquitin ligase by hnRNP-U. Genes Dev **16:**439–451. http://dx.doi.org/10.1101/gad.218702.
49. **Bruss MD, Arias EB, Lienhard GE, Cartee GD.** 2005. Increased phosphorylation of Akt substrate of 160 kDa (AS160) in rat skeletal muscle in response to insulin or contractile activity. Diabetes **54:**41–50. http://dx.doi.org/10.2337/diabetes.54.1.41.
50. **Larance M, Ramm G, Stockli J, van Dam EM, Winata S, Wasinger V, Simpson F, Graham M, Junutula JR, Guilhaus M, James DE.** 2005. Characterization of the role of the Rab GTPase-activating protein AS160 in insulin-regulated GLUT4 trafficking. J Biol Chem **280:**37803–37813. http://dx.doi.org/10.1074/jbc.M503897200.
51. **Sano H, Kane S, Sano E, Miinea CP, Asara JM, Lane WS, Garner CW, Lienhard GE.** 2003. Insulin-stimulated phosphorylation of a Rab GTPase-activating protein regulates GLUT4 translocation. J Biol Chem **278:**14599–14602. http://dx.doi.org/10.1074/jbc.C300063200.
52. **Thong FS, Bilan PJ, Klip A.** 2007. The Rab GTPase-activating protein AS160 integrates Akt, protein kinase C, and AMP-activated protein kinase signals regulating GLUT4 traffic. Diabetes **56:**414–423. http://dx.doi.org/10.2337/db06-0900.
53. **Moltke I, Grarup N, Jorgensen ME, Bjerregaard P, Treebak JT, Fumagalli M, Korneliussen TS, Andersen MA, Nielsen TS, Krarup NT, Gjesing AP, Zierath JR, Linneberg A, Wu X, Sun G, Jin X, Al-Aama J, Wang J, Borch-Johnsen K, Pedersen O, Nielsen R, Albrechtsen A, Hansen T.** 2014. A common Greenlandic TBC1D4 variant confers muscle insulin resistance and type 2 diabetes. Nature **512:**190–193. http://dx.doi.org/10.1038/nature13425.
54. **Colombo SL, Palacios-Callender M, Frakich N, Carcamo S, Kovacs I, Tudzarova S, Moncada S.** 2011. Molecular basis for the differential use of glucose and glutamine in cell proliferation as revealed by synchronized HeLa cells. Proc Natl Acad Sci U S A **108:**21069–21074. http://dx.doi.org/10.1073/pnas.1117500108.
55. **Chu PC, Chuang HC, Kulp SK, Chen CS.** 2012. The mRNA-stabilizing factor HuR protein is targeted by beta-TrCP protein for degradation in response to glycolysis inhibition. J Biol Chem **287:**43639–43650. http://dx.doi.org/10.1074/jbc.M112.393678.
56. **Hodzic DM, Yeater DB, Bengtsson L, Otto H, Stahl PD.** 2004. Sun2 is a novel mammalian inner nuclear membrane protein. J Biol Chem **279:**25805–25812. http://dx.doi.org/10.1074/jbc.M313157200.
57. **Padmakumar VC, Libotte T, Lu W, Zaim H, Abraham S, Noegel AA, Gotzmann J, Foisner R, Karakesisoglou I.** 2005. The inner nuclear membrane protein Sun1 mediates the anchorage of Nesprin-2 to the nuclear envelope. J Cell Sci **118:**3419–3430. http://dx.doi.org/10.1242/jcs.02471.
58. **Yu J, Lei K, Zhou M, Craft CM, Xu G, Xu T, Zhuang Y, Xu R, Han M.** 2011. KASH protein Syne-2/Nesprin-2 and SUN proteins SUN1/2 mediate nuclear migration during mammalian retinal development. Hum Mol Genet **20:**1061–1073. http://dx.doi.org/10.1093/hmg/ddq549.
59. **Lei K, Zhu X, Xu R, Shao C, Xu T, Zhuang Y, Han M.** 2012. Inner nuclear envelope proteins SUN1 and SUN2 play a prominent role in the DNA damage response. Curr Biol **22:**1609–1615. http://dx.doi.org/10.1016/j.cub.2012.06.043.
60. **Tapley EC, Starr DA.** 2013. Connecting the nucleus to the cytoskeleton by SUN-KASH bridges across the nuclear envelope. Curr Opin Cell Biol **25:**57–62. http://dx.doi.org/10.1016/j.ceb.2012.10.014.
61. **Starr DA.** 2012. Laminopathies: too much SUN is a bad thing. Curr Biol **22:**R678–R680. http://dx.doi.org/10.1016/j.cub.2012.06.070.
62. **Kawajiri A, Itoh N, Fukata M, Nakagawa M, Yamaga M, Iwamatsu A, Kaibuchi K.** 2000. Identification of a novel beta-catenin-interacting protein. Biochem Biophys Res Commun **273:**712–717. http://dx.doi.org/10.1006/bbrc.2000.3002.
63. **Sakurai A, Fukuhara S, Yamagishi A, Sako K, Kamioka Y, Masuda M,**

Nakaoka Y, Mochizuki N. 2006. MAGI-1 is required for Rap1 activation upon cell-cell contact and for enhancement of vascular endothelial cadherin-mediated cell adhesion. Mol Biol Cell **17:**966–976. http://dx.doi.org/10.1091/mbc.E05-07-0647.

64. **Skaar JR, Pagano M.** 2009. Control of cell growth by the SCF and APC/C ubiquitin ligases. Curr Opin Cell Biol **21:**816–824. http://dx.doi.org/10.1016/j.ceb.2009.08.004.
65. **Guardavaccaro D, Kudo Y, Boulaire J, Barchi M, Busino L, Donzelli M, Margottin-Goguet F, Jackson PK, Yamasaki L, Pagano M.** 2003. Control of meiotic and mitotic progression by the F box protein beta-Trcp1 in vivo. Dev Cell **4:**799–812. http://dx.doi.org/10.1016/S1534-5807(03)00154-0.
66. **Pannekoek WJ, van Dijk JJ, Chan OY, Huveneers S, Linnemann JR, Spanjaard E, Brouwer PM, van der Meer AJ, Zwartkruis FJ, Rehmann H, de Rooij J, Bos JL.** 2011. Epac1 and PDZ-GEF cooperate in Rap1 mediated endothelial junction control. Cell Signal **23:**2056–2064. http://dx.doi.org/10.1016/j.cellsig.2011.07.022.
67. **Chen EH, Grote E, Mohler W, Vignery A.** 2007. Cell-cell fusion. FEBS Lett **581:**2181–2193. http://dx.doi.org/10.1016/j.febslet.2007.03.033.
68. **Sens KL, Zhang S, Jin P, Duan R, Zhang G, Luo F, Parachini L, Chen EH.** 2010. An invasive podosome-like structure promotes fusion pore formation during myoblast fusion. J Cell Biol **191:**1013–1027. http://dx.doi.org/10.1083/jcb.201006006.
69. **Malassiné A, Cronier L.** 2005. Involvement of gap junctions in placental functions and development. Biochim Biophys Acta **1719:**117–124. http://dx.doi.org/10.1016/j.bbamem.2005.09.019.
70. **Aguilar PS, Baylies MK, Fleissner A, Helming L, Inoue N, Podbilewicz B, Wang H, Wong M.** 2013. Genetic basis of cell-cell fusion mechanisms. Trends Genet **29:**427–437. http://dx.doi.org/10.1016/j.tig.2013.01.011.
71. **Kelley LA, Sternberg MJ.** 2009. Protein structure prediction on the Web: a case study using the Phyre server. Nat Protoc **4:**363–371. http://dx.doi.org/10.1038/nprot.2009.2.
72. **Emsley P, Cowtan K.** 2004. Coot: model-building tools for molecular graphics. Acta Crystallogr D Biol Crystallogr **60**(Pt 12 Pt 1):2126–2132. http://dx.doi.org/10.1107/S0907444904019158.
73. **Freedman TS, Sondermann H, Friedland GD, Kortemme T, Bar-Sagi D, Marqusee S, Kuriyan J.** 2006. A Ras-induced conformational switch in the Ras activator Son of sevenless. Proc Natl Acad Sci U S A **103:**16692–16697. http://dx.doi.org/10.1073/pnas.0608127103.
74. **Boriack-Sjodin PA, Margarit SM, Bar-Sagi D, Kuriyan J.** 1998. The structural basis of the activation of Ras by Sos. Nature **394:**337–343. http://dx.doi.org/10.1038/28548.